Investigation of Structure in the Light Curves of a Sample of Newly Discovered Long Period Variable Stars

Eric R. Craine
Western Research Company, Inc. and GNAT, Inc., 3275 W. Ina Road, Suite 217, Tucson, AZ 85741; send email correspondence to ercraine@wrc-inc.com

Roger B. Culver
Department of Physics, Colorado State University, Fort Collins, CO 80523, and GNAT, Inc.

Richard Eykholt
Department of Physics, Colorado State University, Fort Collins, CO 80523

K. M. Flurchick
Department of Physics, North Carolina Agriculture and Technology University, 1601 E. Market Street, Greensboro, NC, 27411, and GNAT, Inc.

Adam L. Kraus
Department of Astronomy, University of Texas, 2515 Speedway, Stop C1400, Austin, TX 78712, and GNAT, Inc.

Roy A. Tucker
Goodricke-Pigott Observatory, 5500 West Nebraska Street, Tucson, Arizona 85757, and GNAT, Inc.

Douglas K. Walker
Department of Physics and Astronomy, University of Canterbury, New Zealand and GNAT, Inc.

Received February 25, 2015; revised June 30, 2015 and August 24, 2015; accepted September 1, 2015

Abstract Long period variable stars exhibit hump structures, and possibly flares, in their light curves. While the existence of humps is not controversial, the presence of flaring activity is less clear. Mining of a sky survey database of new variable star discoveries (the first MOTESS-GNAT Variable Star Catalog (MG1-VSC)) has led to identification of 47 such stars for which there are sufficient data to explore the presence of anomalous light curve features. We find a number of hump structures, and see one possible flare, suggesting that they are rare events. We present light curves and measured parameters for these stars, and a population statistical analysis.

1. Introduction

Long Period Variable stars (LPVs) have been reported to show anomalous structure in their light curves, in the form of "humps" or shorter duration flares. The nature of these features, and even the reality of the flares, has been a subject of discussion (see, for example, Mais *et al.* 2006). A statistical evaluation of these features is undertaken.

1.1. Long Period Variable stars

Red giant stars that show fairly regular cyclical light curves with periods in the range of 80 to 1,000 days are known as long period variables. Light curve amplitudes are typically > 2.5-magnitude in V, with a smaller change in unfiltered or near infrared bands. Periods can vary between cycles by as much as 10 to 15%. Light curve amplitudes can likewise vary from cycle to cycle. Spectral types are M, S, or C, often exhibiting emission lines resulting from pulsation-driven shock waves interacting with the extended atmospheres.

Several types of light curve activity in LPVs have been recognized and broadly characterized as humps, flares, or micro-variability.

Humps are described (see, for example, Lockwood and Wing 1971), as anomalous increases in brightness of duration typically several tens of days with amplitudes on order 0.1 magnitude or greater at I (1.04), and are fairly common. They are reported by Lockwood and Wing to occur only on the ascending leg of the light curve. The Lockwood and Wing data are sparse and the light curves were sketched by hand, however the existence of the features is convincing. Analysis of Hipparcos data by Melikian (1999) suggest that about 37% of Mira stars in their sample show post-minima humps.

Flares are characterized as short-duration (hours to a day or two) increases in brightness of a few hundredths to many tenths of a magnitude. Schaefer (1991) made a list of 14 candidates, some of which were single observations, and all of which were recognized to be potentially dubious. At best such flares appear to be very rare. Among the most intriguing of the flare mechanisms is one described by Willson and Struck (2001) in which the flare is presumed to be a consequence of interaction between the material outflows of the star and a planet that is being engulfed by the host star.

Micro-variability is discussed in several papers (see, for example, de Laverny *et al.* 1998), and is taken to be short term

(on order 0.1 to 1 day) variation, both positive and negative variations, in excess of Hp ~ .25–1.2 magnitude, predominantly near light curve minimum. The data of de Laverny *et al.* were taken from Hipparcos observations, and in some cases "features" were represented by a single observation. Subsequent studies (Wozniak *et al.* 2004), using the OGLE-II light curves, with less sparse data and photometric accuracy much better than 0.2 magnitude, were unable to confirm the Hipparcos results.

1.2. MG1-VSC

The Global Network of Astronomical Telescopes (GNAT) in collaboration with the Moving Object and Transient Event Search System (MOTESS), is creating new catalogs of variable stars along and within about +12° of the celestial equator. The MOTESS system consists of an array of three conventional Newtonian reflectors with 35-centimeter aperture, f/5 primaries. Imaging is accomplished with thermoelectrically-cooled CCD cameras that are operated in continuous time-delay integration mode. In normal MOTESS operation, the three telescopes are aimed at the same declination but spread in Right Ascension at intervals of 15 to 60 minutes to produce a data stream of image triplets separated in time that reveal moving and time-varying objects; see Tucker (2007).

The time-delay integration (scan mode) imaging allows the telescopes to remain fixed in altitude and azimuth, while the rotation of the Earth continuously scans the established declination band. The telescopes operate each clear night (excepting very bright moon time) from twilight to twilight, yielding an observing cadence of three images per clear night per observing season for each field. The net result is an observing season of four months on and eight months off, with three seasons of data for a 2.5 year survey.

GNAT has also implemented a comprehensive data pipeline for extracting photometric measurements for all of the stars observed in each of the discrete declination bands observed with the scan-mode system. For the first declination band (designated the MG1 Survey), 48 arcminutes wide and centered at $+03^{d}$ 18^{m}, this has resulted in 2.5-year photometric light curves for 2.07 million stars with $-3 < R–B < 5$ and R brighter than 19 magnitude. From these observations a new catalog of variable stars (the *MG1 Variable Star Catalog* (MG1-VSC)) was created. Variable stars numbering 26,042, of which 5,271 are periodic at the 99% confidence level, were found (Kraus *et al.* 2007). Only 59 of these stars were previously known to be variable and appeared as entries in the *General Catalogue of Variable Stars* (GCVS; Kholopov *et al.* 1985).

The MG1 survey is compared with several other photometric sky surveys as shown in Figure 1. The figure shows the survey surface area as a function of limiting magnitude. The surveys are identified for each locus along with a number in parentheses representing the typical number of observations of each field in the survey.

Small, low-cost telescopes can be dedicated to high frequency observations of small areas of sky, such as the Trans-Atlantic Exoplanet Survey (TReS) (Alonso *et al.* 2004), or they can make small numbers of observations of large areas of sky, such as the All-Sky Automated Survey (ASAS) (Pojmański *et al.* 2005). In either case, these surveys have modest magnitude limits because of the small telescope size. Larger aperture telescope surveys can reach much fainter limiting magnitudes, but usually at the expense of less frequent observation or coverage of much smaller areas of the sky, as, for example, the Sloan Digital Sky Survey (SDSS) (York *et al.* 2000) and the Optical Gravitational Lensing Experiment II (OGLE2) (Udalski *et al.* 1997).

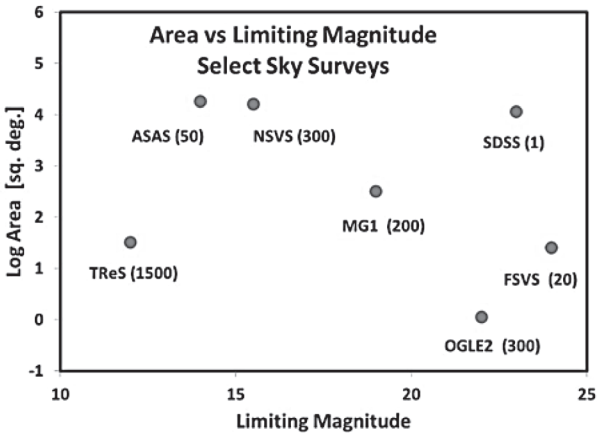

Figure 1. Comparison of coverage area and limiting magnitude for a selection of digital sky surveys including: Sloan Digital Sky Survey (York *et al.* 2000), ASAS (Pojmański *et al.* 2005), Faint Sky Variability Survey (Groot *et al.* 2003), Northern Sky Variability Survey (Wozniak *et al.* 2004), Optical Gravitational Lensing Experiment II (Udalski *et al.* 1997), TReS (Alonso *et al.* 2004), and the MOTESS-GNAT 1 Survey (Kraus *et al.* 2007). The numbers in parentheses are the typical number of times each survey visits a given field.

Examination of the parameter space of Figure 1 indicates that the MG1 survey, better than the other surveys represented, occupies a unique intermediate position in terms of area, limiting magnitude, and observing cadence that is advantageous for stellar variability studies in the field. Other surveys in Figure 1 are more constrained either by limiting magnitude (TReS, ASAS, and NSVS), spatial area (TReS, FSVS, and OGLE2), or by cadence (SDSS).

2. Observational data

The observational data available in the MG1-VSC include a basic data and statistics summary, a file of reduced photometric observations, a light curve plot, and a trial phased light curve. The summary file includes the following: R. A., Dec., light curve amplitude, mean brightness, standard deviation about the mean, photometric error, skew of the observed data points, number of observations, log P (period), and log PFA (period false alarm probability). The brightness measures derived from the MG1 data are an MG1 R magnitude (RMG), as defined in Kraus *et al.* (2007). This magnitude is obtained thorough open channel images yielding the silicon spectral response of the camera. For the long period variable stars discussed in this paper, the photometric errors for each observation typically range from 0.01 to 0.05 mag. Note that for the MG1-VSC compilation, only the A and C MOTESS telescope images were reduced. The B telescope images are also available in the archive. In the event that a potential flare, or other interesting anomalous event, is observed, the B telescope image can also be measured for added clarification.

The period, P, is specified in days and is determined using the Lomb-Scargle method (Lomb 1976; Scargle 1982) as described in Press *et al.* (1992). Because of the telescope spacing, and the interval between nightly observations, short period systems are subject to aliasing. Fortunately, this problem does not impact the LPVs of current interest. The scan mode observations yield an observing season of approximately 4 months' duration, separated by 8-month intervals. A periodogram analysis on a season-by-season basis is then performed. The result is that there can be aliasing for periods of approximately one year as a result of this seasonal cadence. This can lead to confusion in the periods of some LPVs of interest. It is important to recognize that that values of P, and the associated false alarm probability, serve primarily as guides and must be used with extreme caution. For this reason, a new, comprehensive periodogram analysis is computed for all MG1-VSC stars for which we engage in follow-up observation and analysis.

In addition to the MG1-VSC data, United States Naval Observatory (USNO) B magnitude (Monet *et al.* 2003), and J, H, and K magnitudes have been extracted where possible for each of the MG1-VSC stars. The J, H, and K data were taken from 2MASS observations (Skrutskie *et al.* 2006).

3. Data reduction methods

A series of data reduction steps, consisting of manual and automated techniques, were applied to the data set to search for potential flare events, as well as hump-type structures. Steps include visual search for LPV candidates, period determination, and detailed inspection of the resulting suspected flare events.

3.1. LPV identification

The MG1-VSC catalog was initially culled for stars with P > 80 d. This list was then sorted by amplitude and truncated. Rather than truncating the list at 2.5 mag, only very low amplitude variables were deleted. The rationale for this procedure is two-fold: 1) since the MG1 images were unfiltered, the smallest LPV amplitudes are smaller than the 2.5 mag cutoff in V, and 2) to compare this list visually with the corresponding light curves. Visual examination of the remaining light curves was rendered fairly straightforward, since the LPV candidates have very distinctive light curves. The LPV identification process yielded a final list of 47 LPV candidates, for which raw and phased light curves appear in Appendix A.

3.2. Period determination

The MG1-VSC photometric data files for each of the candidate LPVs were then analysed using the ANOVA protocol of the PERANSO period analysis software package (Vanamuster 2014). Systems with periods close to one year (or multiples of one year) were subject to aliasing effects as described above. In these cases, graphical representations of possible phased light curves were constructed, using MATHEMATICA (Wolfram Research, Inc. 2015), to attempt a fit of those peaks in the graphs to computed peak frequencies produced by PERANSO. In most instances a satisfactory period could be distinguished.

In a small number of cases true periodicity is not observable, in the sense that fewer than two complete cycles were observed. This is noted in the data where it occurs. In each instance, the light curve is so distinctively similar to the other LPVs that these stars are also classified as LPVs.

The epoch of maximum brightness for each light curve was obtained either by a direct observation of the maximum brightness epoch or by an estimation of such an epoch. In those cases where the actual maximum epoch could not be directly observed, the epoch Julian date was estimated either by assuming it was located a half period away from the Julian date of an observed minimum light position for a given star or by an interpolation of the star's ascending and descending light curve data.

3.3. Light curve reduction

Selected segments of the datasets, where suspected flaring events were identified, were analyzed as follows:

- A visual inspection was performed on the individual light curves identifying possible flare events.

- The subset of data points surrounding the area of interest was isolated into a separate file.

- A least-square fit to the data points was obtained in order to form a reference line with respect to which distances to individual data points were measured.

- The local slope of the light curve data was "de-trended." This process was performed by generating a perpendicular segment from each data point to the reference line, which yielded the distance of each point off the reference line. The reference line was then redrawn with a slope of zero, with the data points at the appropriate distance from the de-trended line.

- The arithmetic mean of all points in the segment was generated along with standard deviations off the mean. Significant events were indicated by data points lying outside of +2 standard deviations from the mean.

To gain some insights into the limits on the resolution obtainable from the MG1 light curves for possible flares or humps, a series of artificial events was introduced into the light curve data. The flares were set up to have total maximum outbursts of 0.2, 0.1, 0.02, and 0.05 magnitude, with each flare occurring over a total of three days. The flare data were introduced into several light curve regions for which a relatively continuous data stream was available. These segments were tested at all phases of the light curves. The data for each region were de-trended into a horizontal data set, and these de-trended data points were then averaged and the 2-sigma error lines were drawn. From the results of this exercise, it appeared that light curve events having amplitudes of about 0.1 magnitude or larger fall within the limits of detectability, while those with amplitudes equal to or smaller than 0.05 magnitude are not detectable in these light curve data.

When a potential feature is identified, it was characterized as follows. The duration total of each hump feature, in Julian days, was calculated from the value of $t_e - t_b$, where t_e is the

Julian date of the end of a given hump's appearance and t_b is the Julian date of the beginning of the hump's appearance. The Julian date, t_c , of the center of the hump feature was then calculated from $t_c = t_b + 0.5\ t_{total}$. The phase of the center of the event was calculated with respect to the epoch of maximum determined for each light curve.

Because LPVs are well known to have basic periodic light curves for which amplitudes and periods themselves can change by several percent from cycle to cycle, it was important that the above discussed analysis be performed on the raw light curves and not the phased curves. Visual perusal of phased light curves can often "reveal" hump-like features that are not intrinsic humps in the sense used here, but rather artifacts of cycle-to-cycle variations in basic light curve parameters. Hump features reported here are isolated by consistent, objective, statistical considerations applied only to the raw light curves. As such, this method consistently allows detection of more subtle features than visual examination alone, and may lead to higher rates of detection than has otherwise been the case, in part because of increased sensitivity of the approach.

4. Results

Table 1 provides the basic data for the 47 LPV stars under study from the MG1-VSC. The table columns comprise the MG1-serial number (LPV star name), epoch 2000.0 Right Ascension and Declination, the number of observations in the MG1-VSC, the MG1-VSC red magnitude, the period in days, and the Julian date of the epoch of maximum.

Some of the LPV stars in Table 1 were also observed in the 2MASS survey, and J, H, K photometry was obtained. The resulting data are tabulated in Table 2.

Seven clear hump features were identified from the light curve analysis discussed in section 3.3. There are some other light curve segments that are suggestive of the presence of humps, but the data were sufficiently sparse that we have elected not to pursue those features as definitively real. The seven humps identified are shown in Appendix B. These are the de-trended light curve segments, so the magnitude scale for each should be interpreted as a differential magnitude relative to an arbitrary underlying "continuum" mean. Each light curve segment is fit with a high order polynomial to help define the shape of the hump. In two or three cases the hump appears open-ended because it occurred before or after a lapse in observations. The parameters of these features are summarized in Table 3, which lists the star name, the approximate epoch of the hump, the duration of the feature in days, the phase and phase quadrant of the hump event, and the mean magnitude of the event.

A single potential flare event was observed in MG1-1440964 on 5 July 2003, as shown in Figure 2. These data are re-measurements of the MG1 survey images, using all three telescopes. In this case, five sequential nights were measured; the flare event occurred on one night only. Regrettably, this event occurred on the final night of the observing run. This was the only candidate flare that was observed in all three telescopes on the same night, a rigorous criterion we implemented for identifying a real candidate flare.

Table 1. Newly discovered MG1-VSC long period variable stars.

MG1-	*R. A. (2000)*			*Dec. (2000)*			N_{obs}	*R_MG1*	*P*	*Epoch Max.*
	h	*m*	*s*	°	′	″			*(days)*	*JD 2450000+*
1098444	18	02	32	03	05	11	225	14.36	250.0	2594
1117392	18	05	23.8	02	56	36	177	13.65	189.0	2667
1155788	18	10	46.5	02	57	10	218	14.41	181.2	2483
1248064	18	23	34.3	03	24	40	168	13.79	271.0	2370
1258871	18	25	14.7	03	40	25	153	13.51	243.5	2758
1270097	18	26	54.7	02	54	38	168	13.70	232.9	2785
1270289	18	26	56.6	03	13	16	149	13.62	152.8	2455
1287551	18	29	35	03	28	14	128	13.53	424.8	2632
1291327	18	30	10.4	03	23	30	129	13.40	238.8	2818
1315064	18	35	21.7	03	38	18	103	13.32	292.9	2665
1326286	18	37	45	03	39	23	208	14.62	297.6	2623
1334111	18	39	19.7	03	03	04	194	14.38	294.9	2629
1334664	18	39	26.7	03	16	42	151	14.23	292.9	2642
1336304	18	39	47.9	03	05	19	204	13.96	348.0	2357
1339600	18	40	33.7	03	25	50	205	15.29	331.7	2553
1341934	18	41	14.6	03	20	06	188	14.21	232.3	2750
1344747	18	42	03.5	03	05	54	207	14.31	190.3	2455
1372707	19	04	25.4	03	25	17	153	15.51	343.6	2573
1375418	19	04	51.9	02	54	16	198	15.12	541.6:	2518
1376419	19	05	01.1	03	10	19	133	15.22	320.0	2604
1379672	19	05	30.1	03	33	20	147	13.49	151.1	2788
1388413	19	06	41.4	03	02	17	109	13.36	234.0	2569
1388633	19	06	43.1	03	17	12	145	13.65	188.2	2790
1391053	19	06	58.5	02	59	14	185	14.11	432.0	2676
1393846	19	07	16	02	57	34	173	13.67	365.5	2817
1406788	19	09	17.3	02	54	52	132	13.49	296.5	2648
1410394	19	09	48	03	34	30	170	13.73	176.7	2794
1410977	19	09	53	02	54	21	169	13.40	344.7	2699
1413873	19	10	16.1	03	01	58	199	14.76	347.5	2348
1414532	19	10	21.2	02	58	05	151	13.39	306.5	2794
1428501	19	12	07.2	03	03	11	118	13.55	215.7	2497
1440964	19	13	59.4	03	07	44	165	13.70	427.1	2697
1444065	19	14	26.9	03	11	18	125	13.89	258.7	2434
1448319	19	15	03.2	02	55	05	186	13.64	210.8	2797
1457857	19	16	17.3	03	37	02	149	13.07	271.3	2463
1466778	19	17	31.5	03	23	08	127	13.65	298.2	2642
1468465	19	17	45.7	02	55	39	166	14.80	167.3	2579
1477416	19	19	00.1	03	30	46	121	13.37	137.8	2427
1478012	19	19	05.2	03	24	33	185	16.44	353.2	2760
1492532	19	21	09.3	03	32	06	183	14.14	204.2	2775
1496600	19	21	50.1	03	31	04	78	13.32	272.8	2439
1518640	19	24	49.1	03	37	21	81	13.06	226.0	2640
1523972	19	25	30.5	03	18	32	159	13.86	265.3	2636
1540903	19	27	36.9	03	23	11	137	13.69	266.6	2430
1545107	19	28	08.1	03	00	26	189	14.65	520.8	2460
1653368	19	42	25.2	03	32	01	137	13.60	228.0	2430
1877036	20	28	46.8	02	59	06	169	14.15	171.2	2520

Table 2. 2MASS infrared photometry.

MG1-	*J*	*J–H*	*H–K*	*MG1-*	*J*	*J–H*	*H–K*
1248064	14.287	0.454	0.292	1440964	9.563	1.247	0.834
1258871	9.644	0.931	0.646	1444065	8.827	1.079	0.634
1270289	8.851	0.931	0.552	1457857	12.486	0.463	0.104
1287551	7.082	1.313	1.06	1466778	9.461	1.166	0.789
1291327	9.623	0.964	0.562	1477416	10.686	0.888	0.686
1315064	9.369	1.094	0.724	1492532	13.647	0.755	0.228
1326286	9.071	1.209	0.624	1496600	9.176	1.004	0.674
1334664	13.938	1.037	0.324	1518640	7.997	0.974	0.568
1339600	14.9	0.82	0.454	1523972	10.011	0.881	0.552
1341934	9.679	1.246	0.626	1540903	9.791	0.894	0.538
1372707	9.888	1.524	0.925	1545107	9.826	1.643	1.277
1379672	9.619	1.13	0.504	1653368	10.126	0.885	0.576
1388633	10.165	1.062	0.562	1877036	11.449	0.842	0.409
1410394	9.569	1.092	0.612				

Table 3. LPV hump statistics.

MG1-	*Approximate Hump Center JD 2450000+*	*Approximate Duration (days)*	*Phase (del t)/P*	*Phase Segment**	*Amplitude (magnitude)*
1098444	2458	15	0.46	3	0.1
1258871	2785	46	0.11	1	0.2
1291327	2460	>20	0.50	3	0.1
1334111	2455	20	0.41	3	0.1
1339600	2775	86	0.67	4	0.4
1341934	2438	45	0.66	4	0.1
1414532	2390	>40	0.68	4	0.1

**Phase quadrants: 1, maximum; 2, descending; 3, minimum; and 4, ascending.*

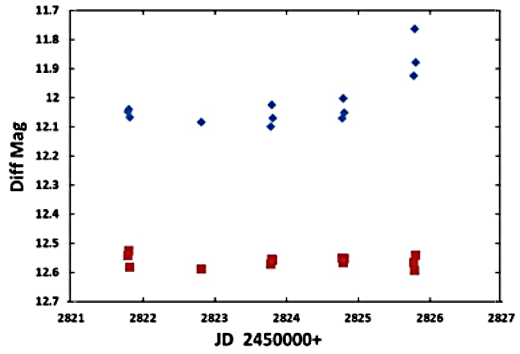

Figure 2. A possible flare event in MG1-1440964 (diamonds); compared with a field check star (squares). The differential magnitudes have been arbitrarily scaled to magnitude 12.0 for the check star. The flare event lies entirely outside the 2-sigma limits around the mean magnitude of the star.

5. Discussion

In this section, the probability for observing a flare in a set of observations is derived. For long period variable stars, the observations can have large observing gaps, so a statistical analysis for the probability of observing a flare is derived. This normalized probability is a function of the average time for a flare to occur, and the observing time.

To begin, define the finite probability, P(Δt), for a flare to occur in a short time, Δt, as:

$$P(\Delta t) = \alpha\, \Delta t \tag{1}$$

where α is the probability per unit time for a flare to occur. In the limit, as Δt goes to zero, Equation 1 becomes exact.

The probability for a flare not occurring in a short time, Δt, is simply:

$$\tilde{P}(\Delta t) = 1 - P(\Delta t) \cong 1 - \alpha\, \Delta t \tag{2}$$

Then, for a long time (that is, a large number of finite time intervals t = N Δt), the probability that a flare does not occur is given by:

$$\tilde{P}(t) \cong [\tilde{P}(\Delta t)]^N \cong (1 - \alpha\, \Delta t)^N \cong (1 - \frac{\alpha t}{N})^N \tag{3}$$

and the exact probability that a flare does not occur during a time t is:

$$\tilde{P}(t) = \lim_{n\to\infty} (1 - \frac{\alpha t}{N})^N = e^{-\alpha t} \tag{4}$$

Now, the exact probability for a flare not to occur until time t, but to occur during the next time interval dt, is the product of the probability of the flare not occurring during the time t and the flare occurring in the infinitesimal time step dt:

$$\mathcal{P}(t) = \tilde{P}(t)\, P(dt) = e^{-\alpha t}\, \alpha dt \tag{5}$$

Therefore, the average time for a flare to occur, T_0, is simply:

$$T_0 = \int_0^\infty \mathcal{P}(t)\, t\, dt = \alpha \int_0^\infty t\, e^{-\alpha t}\, dt = \alpha^{-1} \tag{6}$$

which gives $\alpha = 1/T_0$, and, finally, the exact probability for a flare not to occur during an observing time t is:

$$\tilde{P}(t) = e^{-t/T_0} \tag{7}$$

If the duration of a flare is τ_0, then observing for a time τ will rule out a flare starting during an observation time interval $\tau + \tau_0$. This is the observation gap time. Thus, observation gaps need to be reduced by τ_0, but not become less than zero. The total observation time biased by the occurrence of a flare, can be found as follows:

1. Find the total observing time. Subtract the start time of the first observation from the end time of the final observation (the observing time).

2. Subtract the reduced gap time from Eqn. 1 and add τ_0.

3. Combine these results for all stars, denoted as the total observation time t.

The total observation time, biased by the reduced gap time, gives the probability of not seeing flares in these observations. This can be expressed as in Equation 7. Using this approach, we can hypothesize detectible flare intervals and flare durations for each star in our sample, as shown in Table 4, and calculate the probability that in each case we would not observe at least one flare event in the ensemble.

The one possible flare event observed was at the end of the observing cycle, and so cannot be confirmed as a flare. This leaves us in an ambiguous position with regard to flare events, and supports the conclusion that such features are likely quite rare.

Table 4. Probabilities of observing no flares for the LPV observations.

Flare Interval (years)	*Flare Duration (days)*			
	0.25	0.5	1	2
	Probability			
0.5	0.00174	1.20E-06	3.10E-12	1.20E-15
1	0.0292	0.0011	1.80E-06	3.50E-08
2	0.171	0.0328	0.0013	1.90E-04
3	0.3079	0.1025	0.0121	0.0033
5	0.4934	0.2549	0.0708	0.0323

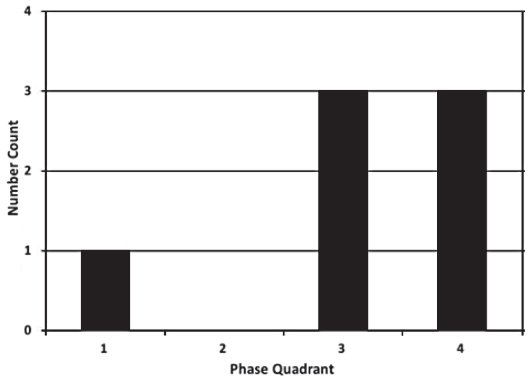

Figure 3. Frequency count of hump features as a function of phase segment; segment 1 is centered at maximum, 2 is the descending leg, 3 is centered at minimum; and 4 is the ascending leg.

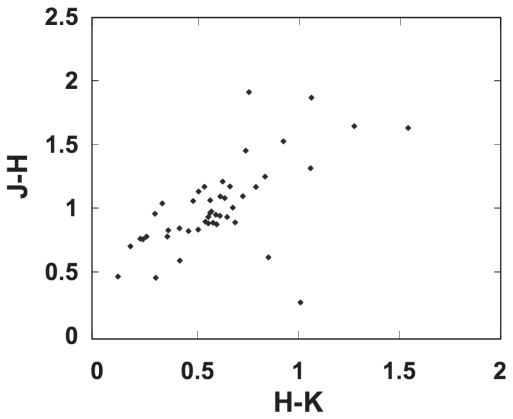

Figure 4. This is the (J–H) vs (H–K) color-color diagram for the LPV candidates that were extracted from the MG1-VSC.

The hump feature distributions as a function of light curve phase can be evaluated, as shown in Figure 3. They predominate at minimum and on the ascending leg, though these are statistics of small numbers.

The (J–H) and (H–K) colors of these stars are plotted in Figure 4. The locus of these observations is consistent with the interpretation that these stars are of spectral types M, S, or C (Cox 2000).

6. Conclusions

The conclusions of this program may be summarized as follows:

• The MG1-VSC catalog is a productive source of LPV discoveries and yields additional data on anomalous light curve features.

• The cadence of MG1-VSC observations allows good definition of hump features and is equivalent to, or superior to, the hump sensitivity in most other reports of such features.

• Unlike visual examination of LPV light curves for hump features used in the literature cited earlier, this paper presents an objective mathematical algorithm for detecting and characterizing the hump features.

• Hump structures are relatively common, and appear to be somewhat preferentially distributed across specific phases of variability. Unlike reports of Lockwood and Wing (1971) and others, we see hump features across a broader range of light curve phase, including not only ascending legs but also during minima and maxima. We saw no hump features on descending legs.

• High temporal resolution allowed reasonably accurate constraints on the range of durations of hump features. In the data reported here hump durations ranged from about 15 to 90 days. This is an average of 0.14P with a standard deviation of 0.04P, where P is the mean variable period in days.

• Based on these stars from the MG1-VSC, short period flares appear to be rare at best, but there is an indication that some may exist in the collective MG surveys. A rigorous statistical analysis is presented to set limits on flare detection using the MG1-VSC data.

Future work includes mining other MG-VSC catalogs, with follow-on observations of some of the current candidate stars.

7. Acknowledgements

This research has made use of the SIMBAD database, operated at CDS, Strasbourg, France. We appreciate a grant from Dr. Janice Nerger, Dean of the College of Natural Sciences, Colorado State University, Fort Collins, Colorado, for computer resources to apply to GNAT research projects.

References

Alonso, R., *et al.* 2004, *Astrophys. J.*, **613**, L153.

Cox, A. N. 2000, *Allen's Astrophysical Quantities*, 4th ed., Springer, New York.

de Laverny, P., Mennessier, M., Mignard, F., and Mattei, J. 1998, *Astron. Astrophys.*, **330**, 169.

Groot, P. J., *et al.* 2003, *Mon. Not. Roy. Astron. Soc.*, **339**, 427.

Kholopov, P. N., *et al.* 1985, *General Catalogue of Variable Stars*, 4th ed., Moscow.

Kraus, A. L., Craine, E. R., Giampapa, M. S., Scharlach, W. W. G., and Tucker, R. A. 2007, *Astron. J.*, **134**, 1488.

Lockwood, G. W., and Wing, R. F. 1971, *Astrophys, J.*, **169**, 63.

Lomb, N. R. 1976, *Astrophys. Space Sci.*, **39**, 447.

Mais, D. E., Richards, D., and Stencel, R. E. 2006, *The Society for Astronomical Sciences 25th Annual Symposium on Telescope Science* (May 23–25, 2006), Society for Astronomical Sciences, Rancho Cucamonga, CA, 31.

Melikian, N. 1999, *Astrophys.*, **42**, 408.

Monet, D., *et al.* 2003, USNO-B V2.0 Catalog, *Astron. J.*, **125**, 984.

Pojmański, G., Pilecki, B., and Szczygiel, D. 2005, *Acta Astron.*, **55**, 275.

Press, W. H., Teukolsky, S. A., Vetterling, W. T., and Flannery, B. P. 1992, *Numerical Recipes in FORTRAN*, Cambridge Univ. Press, Cambridge.

Scargle, J. D. 1982, *Astrophys. J.*, **263**, 835.

Schaefer, B. 1991, *Astrophys. J.*, **366**, L39.
Skrutskie, M. F., *et al.* 2006, The Two Micron All Sky Survey, *Astron. J.*, **131**, 1163.
Tucker, R. A. 2007, *Astron. J.*, **134**, 1483.
Udalski, A., Kubiak, M., and Szymanski, M. 1997, *Acta Astron.*, **47**, 319.
Vanmunster, T. 2014, Light Curve and Period Analysis Software, PERANSO v.2.50 (http://www.peranso.com/).
Willson, L. A., and Struck, C. 2001, *J. Amer. Assoc. Var. Star Obs.*, **30**, 23.
Wolfram Research, Inc. 2015, MATHEMATICA software (http://www.wolfram.com/mathematica/).
Wozniak, P. R., *et al.* 2004, *Astron. J.*, **127**, 2436.
York, D. G., *et al.* 2000, *Astron. J.*, **120**, 1579.

Appendix A. Raw and phased light curves for MG1-VSC LPVs

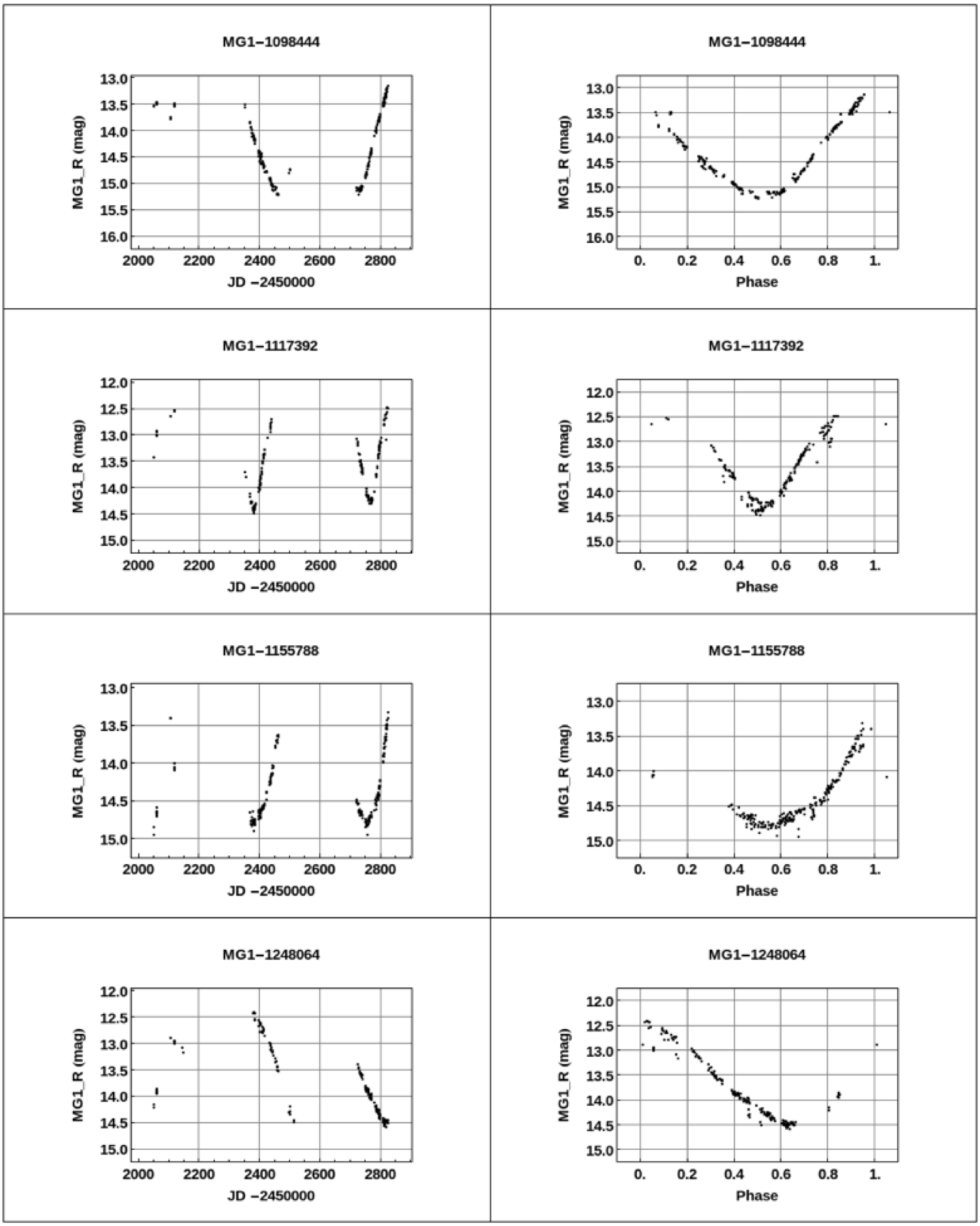

Figure 5. Raw and phased light curves for MGI-VSC LPVs (figure continued on following pages).

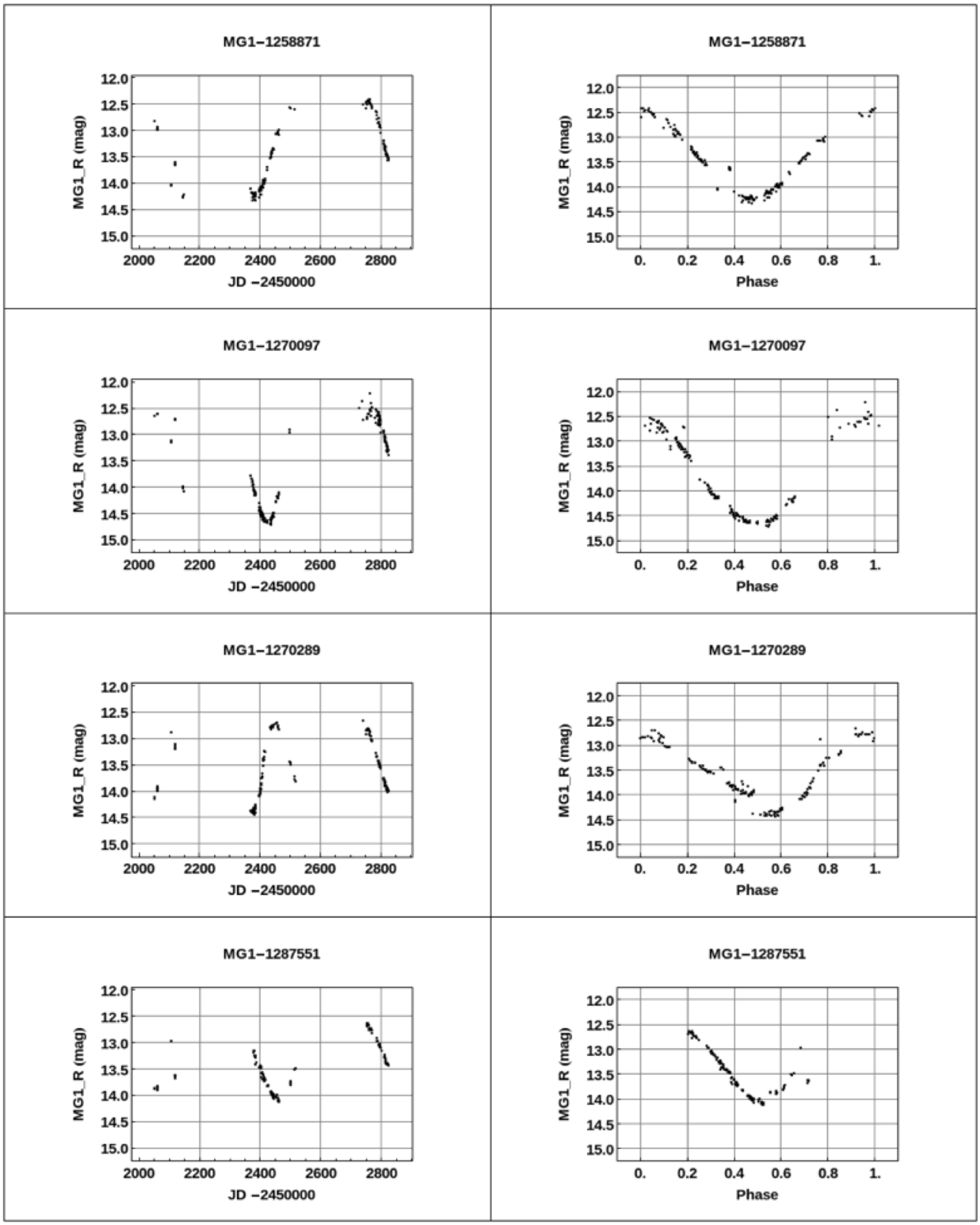

Figure 5. Raw and phased light curves for MGI-VSC LPVs, continued.

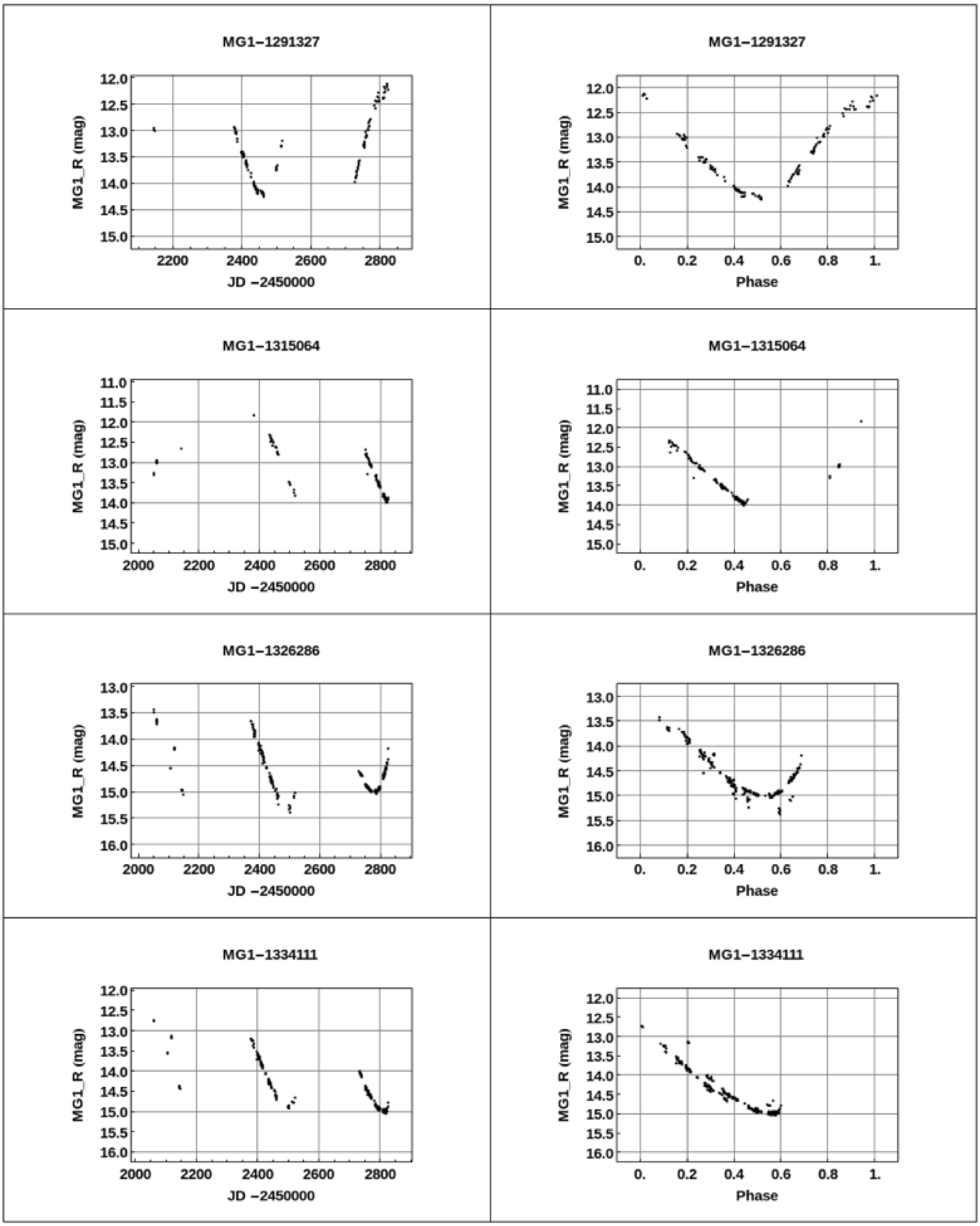

Figure 5. Raw and phased light curves for MGI-VSC LPVs, continued.

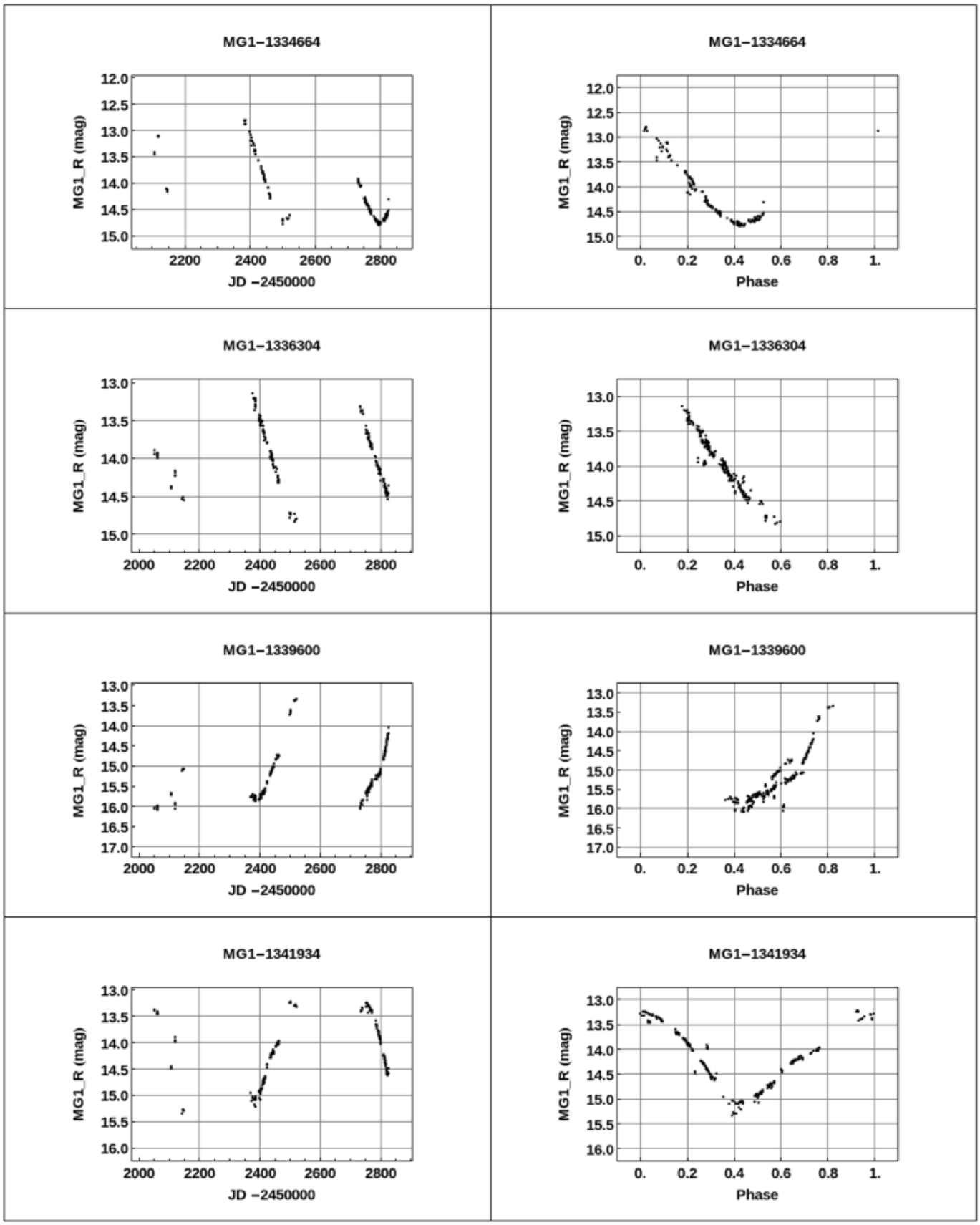

Figure 5. Raw and phased light curves for MGI-VSC LPVs, continued.

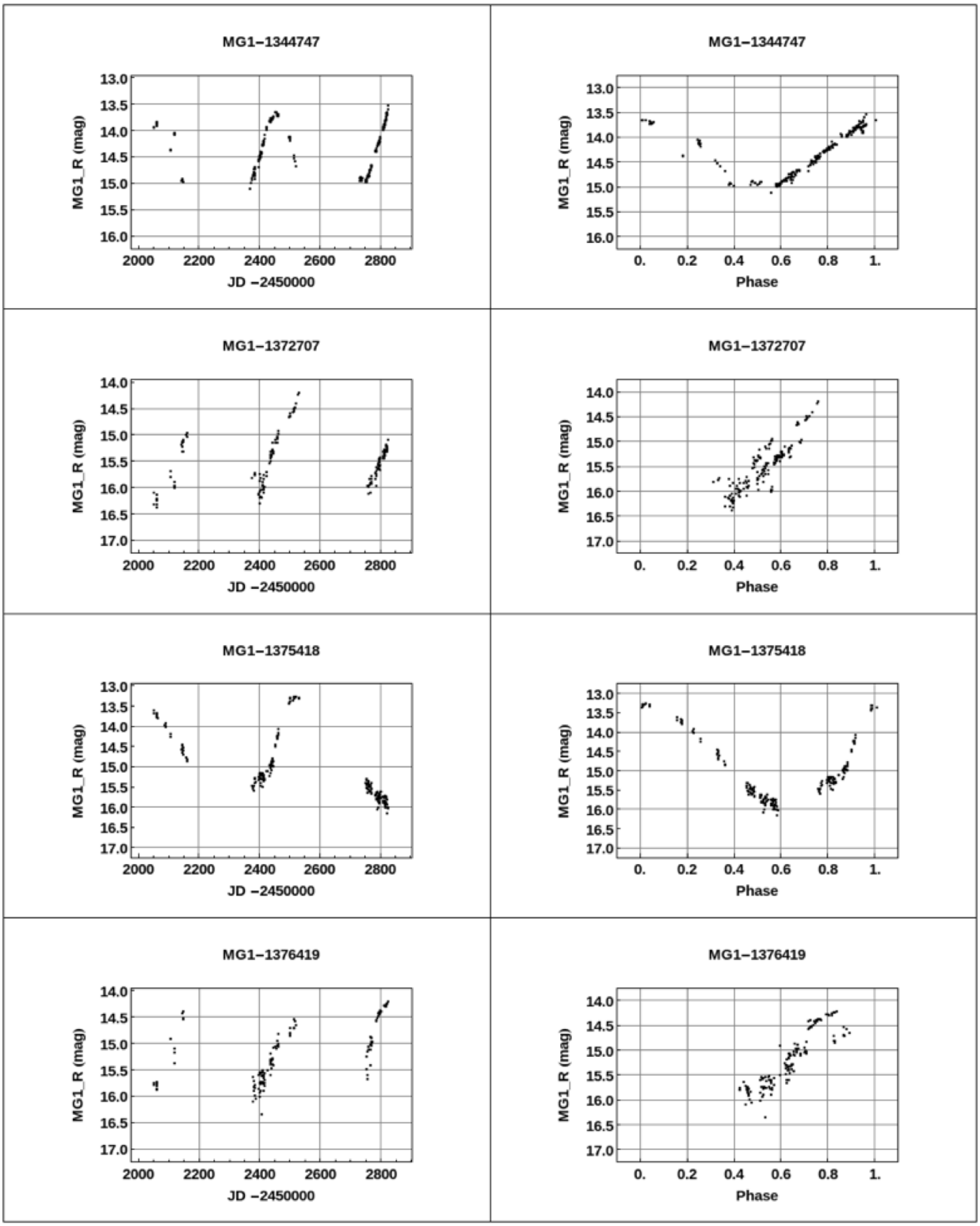

Figure 5. Raw and phased light curves for MGI-VSC LPVs, continued.

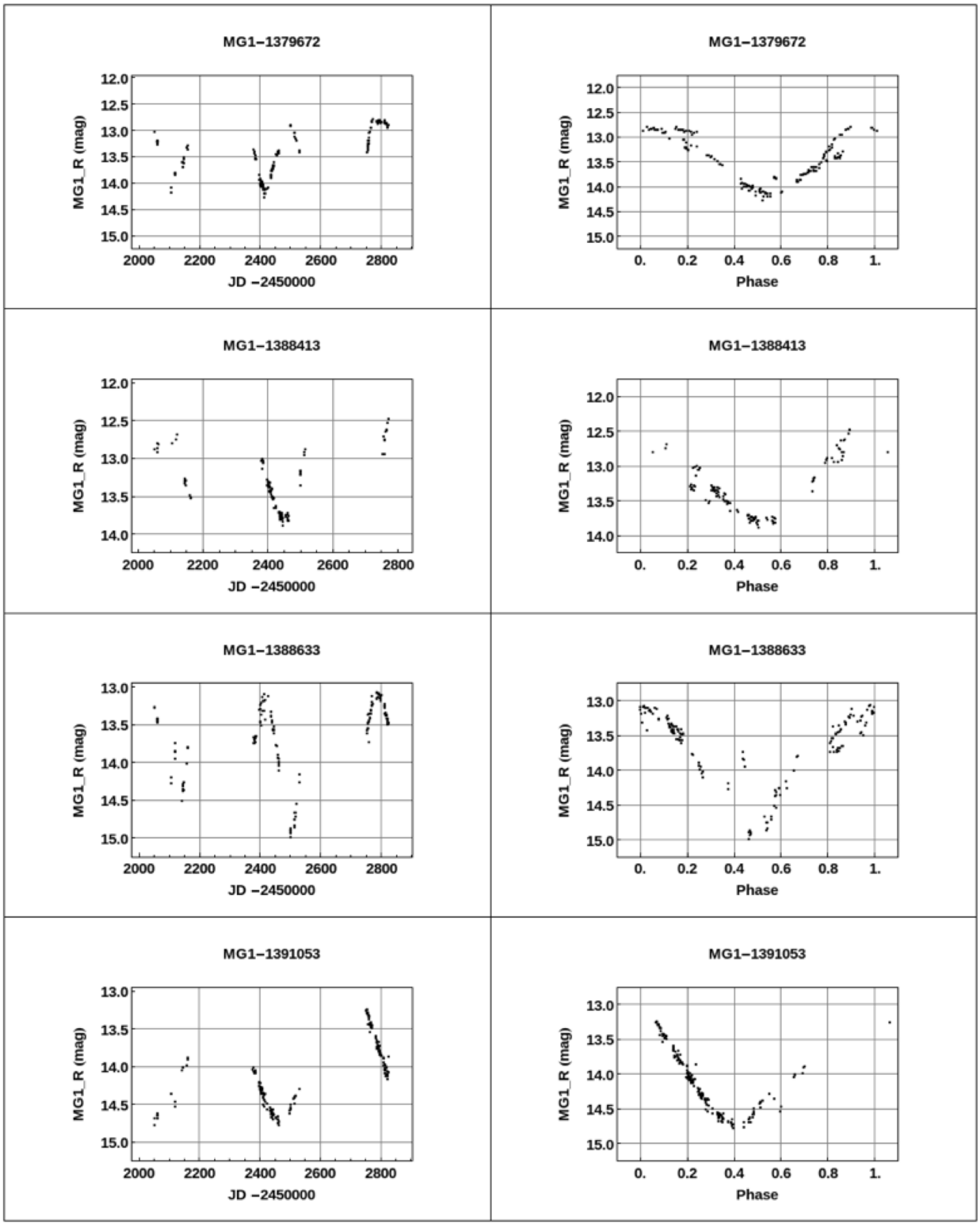

Figure 5. Raw and phased light curves for MGI-VSC LPVs, continued.

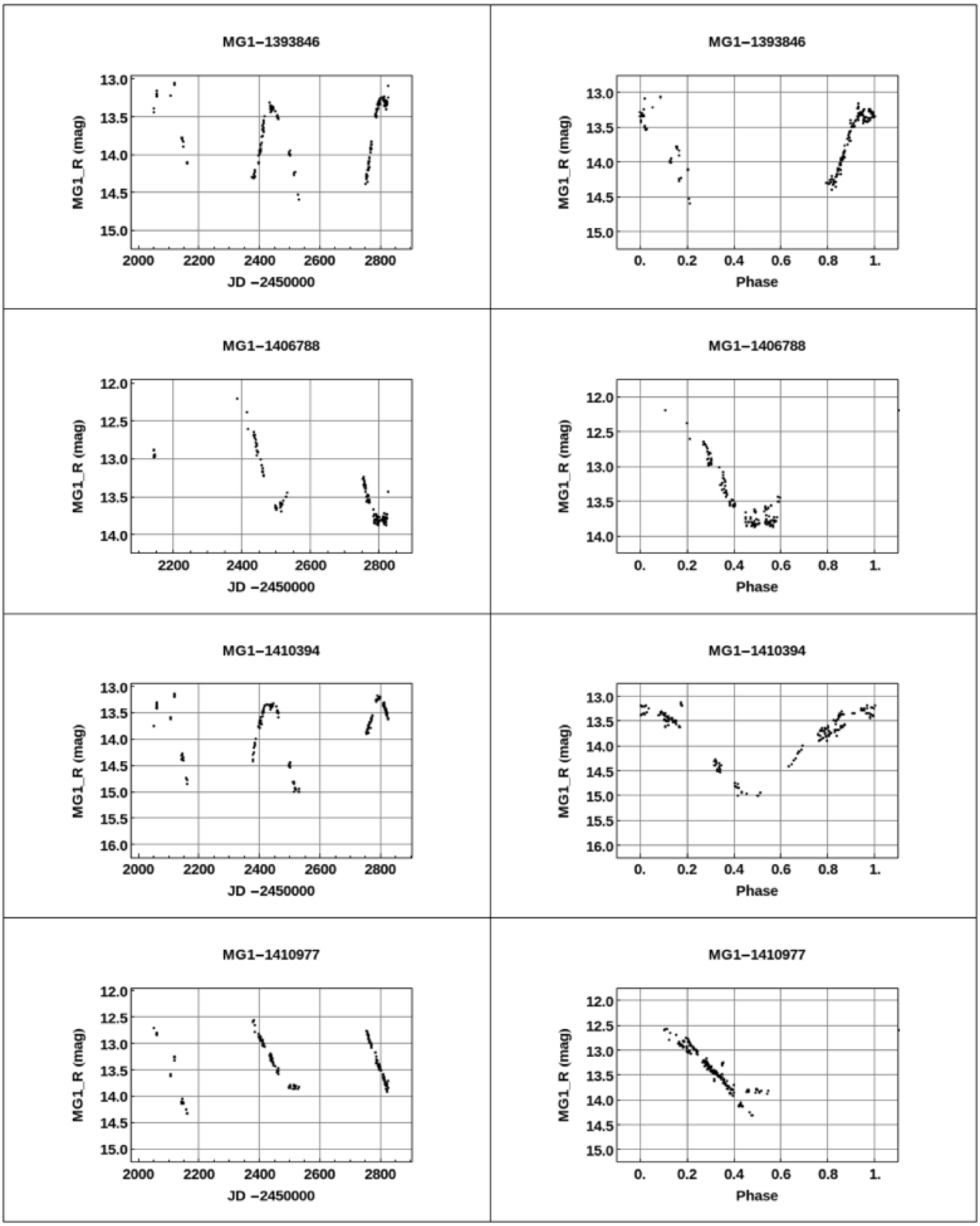

Figure 5. Raw and phased light curves for MGI-VSC LPVs, continued.

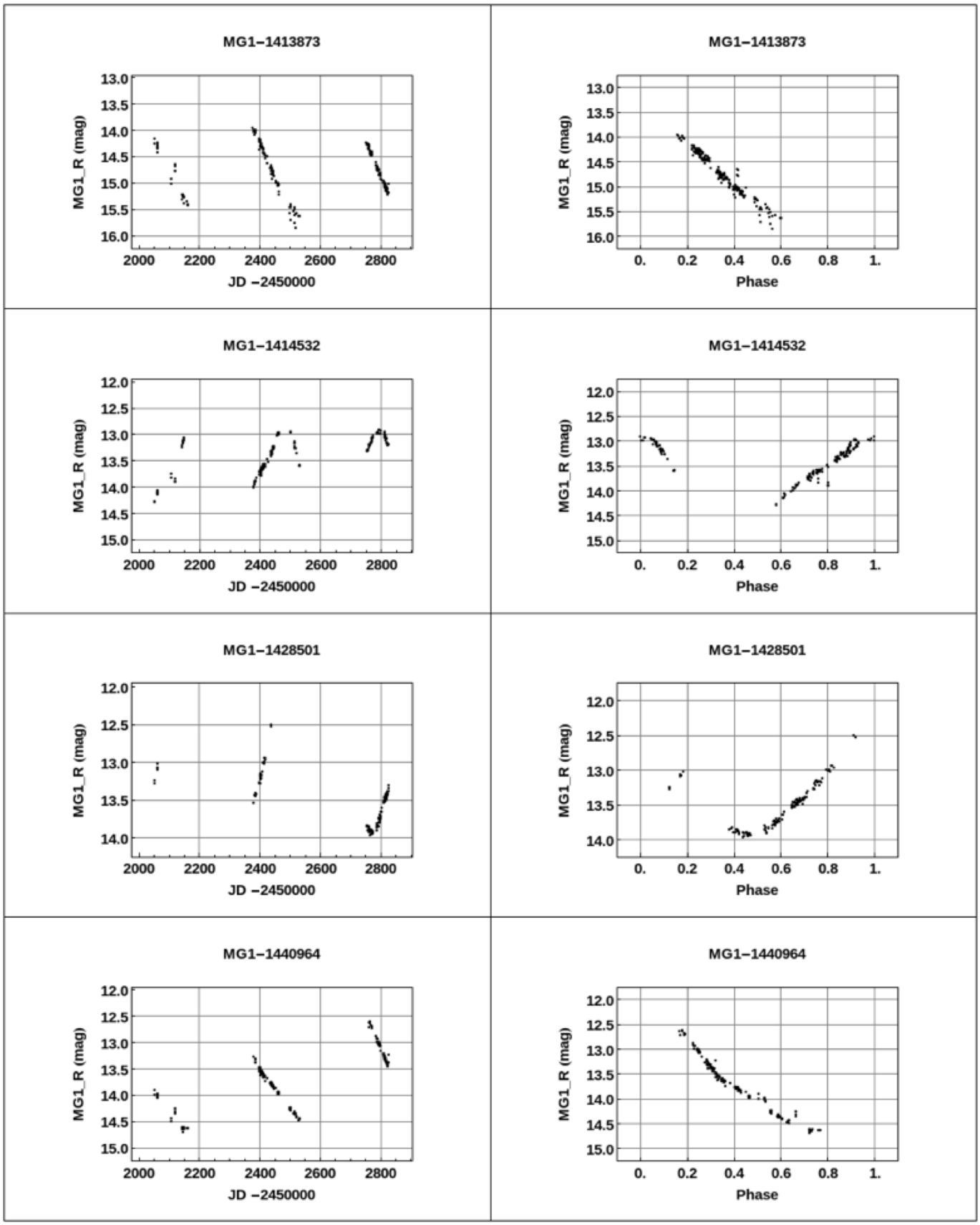

Figure 5. Raw and phased light curves for MGI-VSC LPVs, continued.

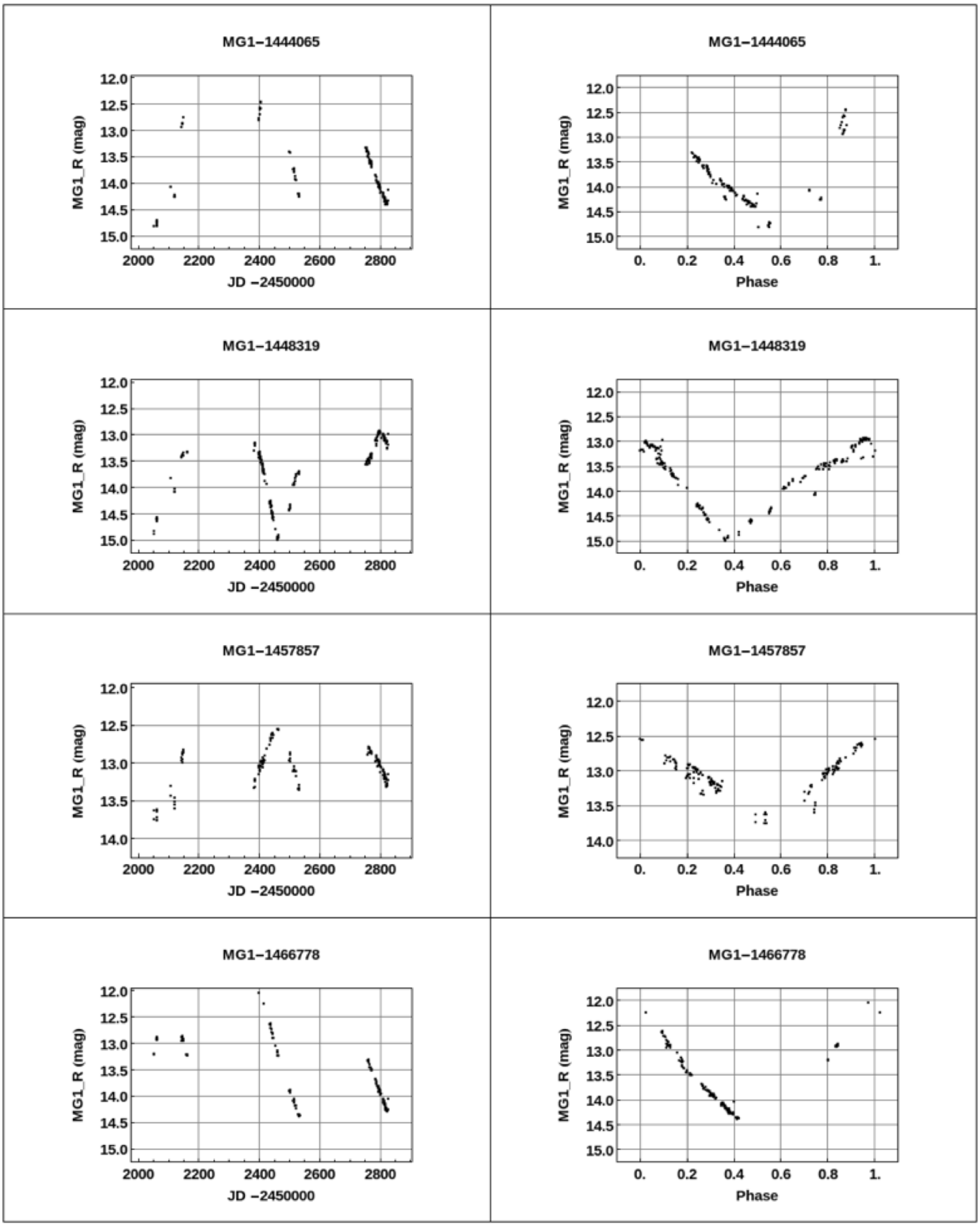

Figure 5. Raw and phased light curves for MGI-VSC LPVs, continued.

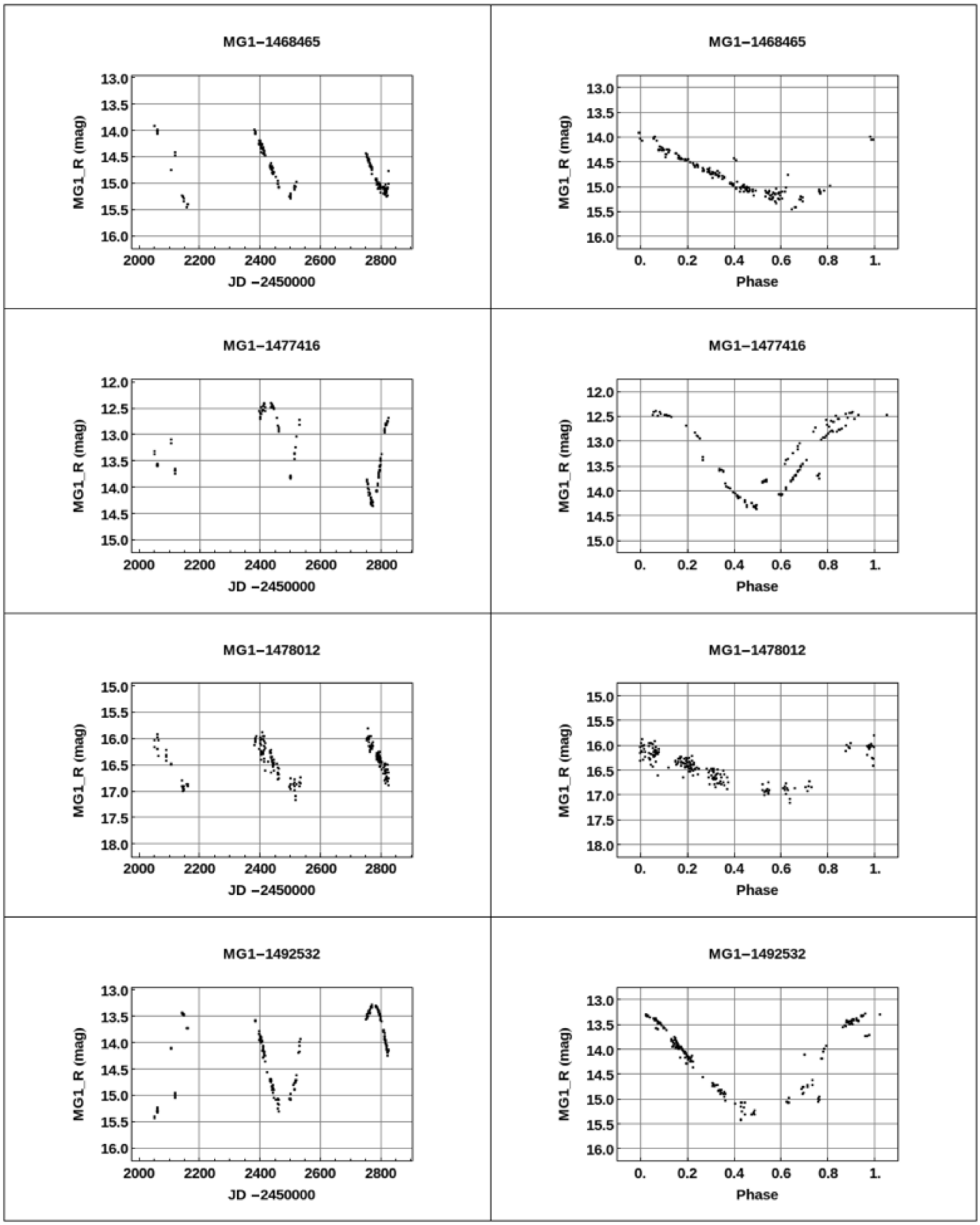

Figure 5. Raw and phased light curves for MGI-VSC LPVs, continued.

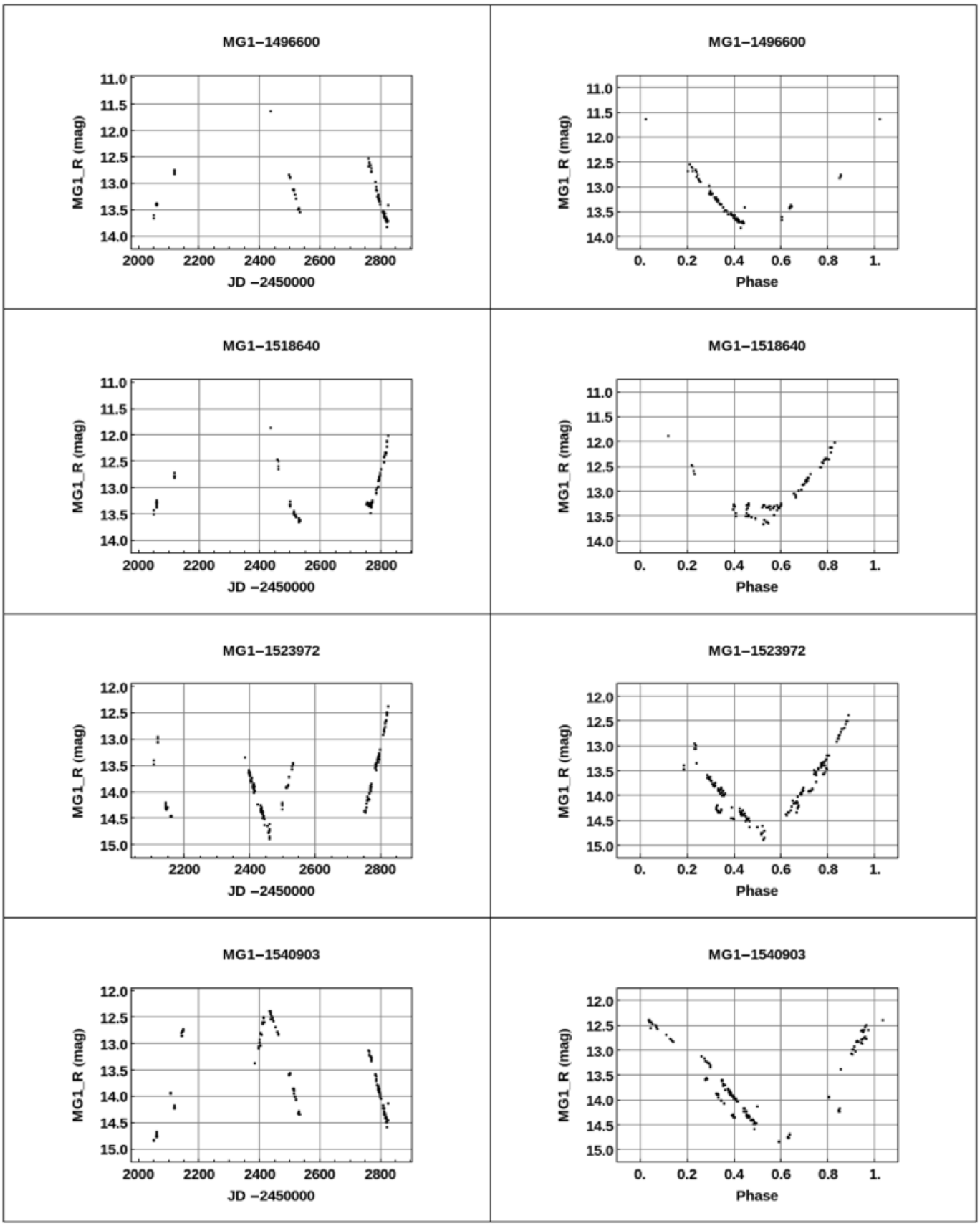

Figure 5. Raw and phased light curves for MGI-VSC LPVs, continued.

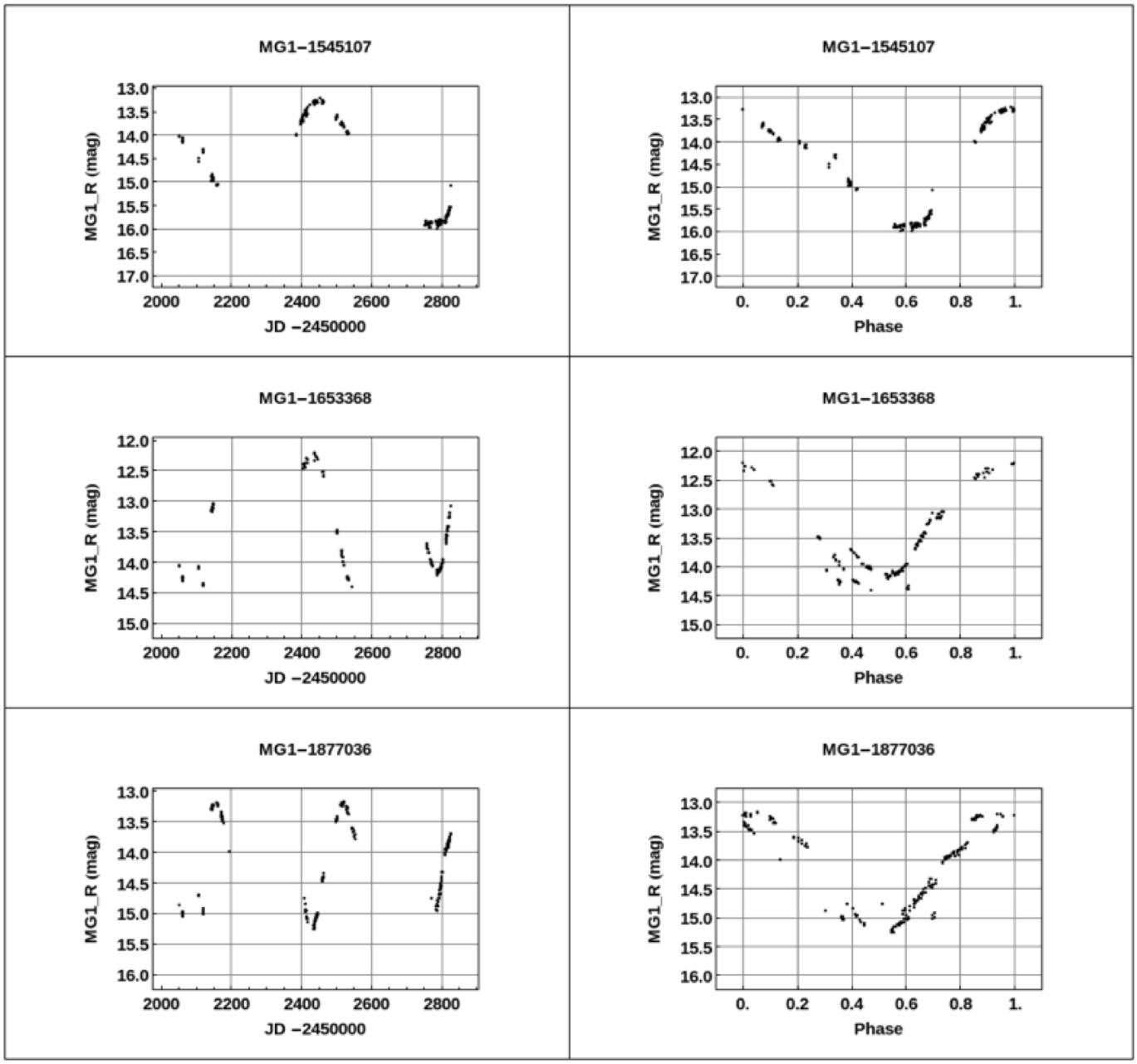

Figure 5. Raw and phased light curves for MGI-VSC LPVs, continued.

Appendix B. Hump features in light curves of MG1-VSC LPVs

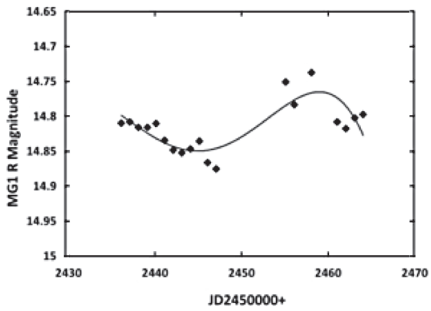

Figure 6a. Hump features in light curve of MG1-1098444.

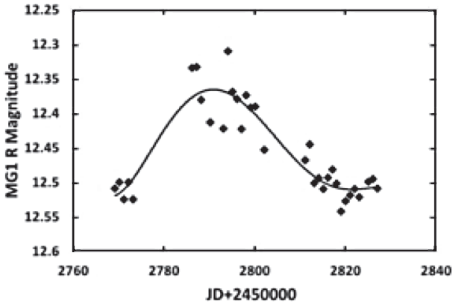

Figure 6b. Hump features in light curve of MG1-1258871.

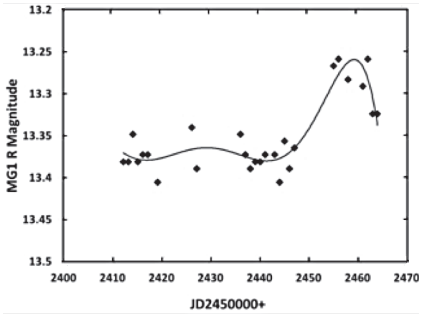

Figure 6c. Hump features in light curve of MG1-1291327.

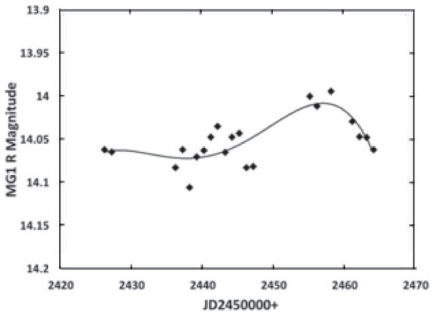

Figure 6d. Hump features in light curve of MG1-1334111.

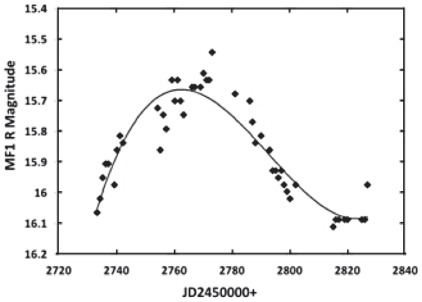

Figure 6e. Hump features in light curve of MG1-1339600.

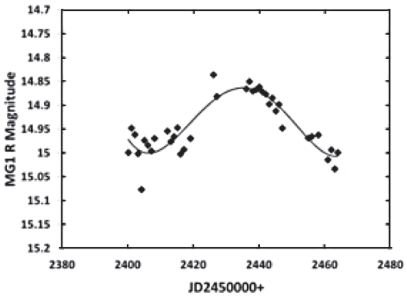

Figure 6f. Hump features in light curve of MG1-1341934.

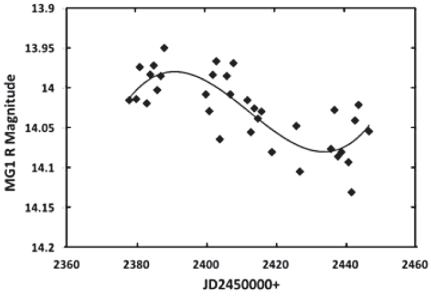

Figure 6g. Hump features in light curve of MG1-1414532.